Tectonophysics 656 (2015) 52–60

Contents lists available at ScienceDirect

Tectonophysics

journal homepage: www.elsevier.com/locate/tecto

Aseismic strike–slip associated with the 2007 dike intrusion episode in Tanzania

Yuji Himematsu *, Masato Furuya [1]

Department of Natural History Sciences, Hokkaido University, N10W8, Kita-ku, Sapporo 060-0810, Japan

ARTICLE INFO

Article history:
Received 10 February 2015
Received in revised form 1 June 2015
Accepted 2 June 2015
Available online 14 June 2015

Keyword:
East African Rift valley
InSAR
Aseismic slip
Transfer zone
Relay ramp
Dike intrusion

ABSTRACT

In July 2007, an earthquake swarm initiated in northern Tanzania near Lake Natron and lasted for about two months. Mt. Oldoinyo Lengai, located to the southwest of the swarm, began to erupt effusively about a month prior to the swarm, and increased its eruption intensity on September when the swarm almost ceased. Several previous studies have already reported the crustal deformation signals associated with the swarm using Interferometric Synthetic Aperture Radar (InSAR). However, nearly all the published data are based on the C-band ENVISAT/ASAR images acquired only from the descending path. We use the L-band ALOS/PALSAR images acquired from both ascending and descending paths, which allow us to examine the deformation signals in more detail. In addition to the InSAR data, we employ the offset-tracking technique to detect the signals along the azimuth direction. Using InSAR and offset-tracking data, we obtain the full 3D displacement fields associated with the episode. Besides the horizontal extension and subsidence signals due to the dike intrusion as already reported, the inferred full 3D displacements further indicate that the subsiding zone was horizontally moving by ~48 cm toward SSW. To explain the displacements, we performed fault source modeling, assuming an elastic half space. The fault slip distribution indicates that the contribution of the strike–slip component is about 20% of total moment release. Because almost all the focal mechanisms of earthquakes during the 2007 event indicate nearly pure normal faulting, aseismic strike–slip must have been responsible for the horizontal movement of the subsiding zone. The strike–slip at the shallowest depths suggests the presence of transtensive stress, which seems to be reasonable to generate the relay zones that are widely observed in the East African Rift. We also confirmed that the stress changes due to the dike intrusion were consistent with the inferred fault slip distributions.

1. Introduction

The East African Rift (EAR) valley is a divergent plate boundary between Nubian plate and Somalian plate that extends the length of ~5000 km-long from Ethiopia to Mozambique (e.g., Ebinger, 1989; McKenzie et al., 1970). The EAR contains numerous normal faults and Quaternary active volcanoes along the rift (e.g., Hamling et al., 2009; Paquet et al., 2007). Also, moderate-sized earthquakes frequently occur along the plate boundary (e.g., Chorowicz, 2005).

Northern Tanzania is located in the middle of the EAR, and the relative opening rate is 2–4 mm/yr along the E–W direction according to the GPS measurement (Saria et al., 2014; Stamps et al., 2008).

The 2007 swarm near the Lake Natron started on July 12 (e.g., Calais et al., 2008). The largest earthquake with moment magnitude (Mw) 5.9 occurred on July 17, and the swarm activity continued until the middle of September 2007 (Fig. 1). The campaign-based local seismic network revealed the details of spatial–temporal distribution of epicenters, indicating a migration of earthquake swarm from a deeper depth to the SW toward a shallower depth in the NE (Albaric et al., 2010). Albaric et al. (2010) and Global CMT catalogue (http://www.globalcmt.org) reported that eight earthquakes with magnitude larger than 5 occurred during the event, all of which indicated ENE–WSW striking normal fault at depths shallower than 20 km. A swarm of more 1400 earthquakes was recorded for 180 days by a campaign seismic network since June 1 (Albaric et al., 2010).

Earthquake swarms are often accompanied with magma intrusion (e.g., Aoki et al., 1999). Mt. Oldoinyo Lengai located about 20 km to the SW from the swarm, is one of the most active volcanoes along the EAR. In 2007, an effusive eruption started one month prior to the swarm activity for the first time in 24 years. The eruptive activity of Mt. Oldoinyo Lengai abruptly switched to episodic explosive eruptions when the swarm activity was decaying in September and continued until April 2008.

Several previous studies have already reported the crustal deformation signals associated with the swarm by using satellite synthetic aperture radar (SAR) data (Baer et al., 2008; Biggs et al., 2009; Calais et al., 2008). Calais et al. (2008) pointed out the presence of aseismic slow slip

* Corresponding author. Tel.: +81 11 706 3527.
E-mail addresses: hime.matsu@frontier.hokudai.ac.jp (Y. Himematsu), furuya@mail.sci.hokudai.ac.jp (M. Furuya).
[1] Tel.: +81 11 706 2759.

http://dx.doi.org/10.1016/j.tecto.2015.06.005
0040-1951/

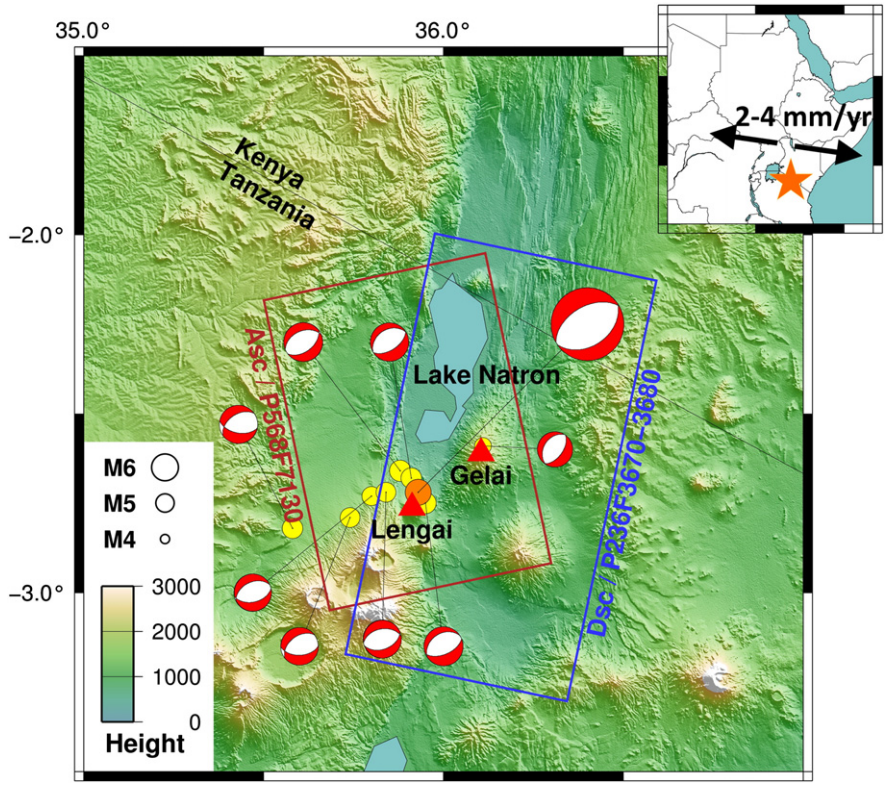

Fig. 1. Our study area is located to the south of Lake Natron, Northern Tanzania, near the Kenyan border (upper-right map). Yellow circles and beach balls show the earthquake epicenters and focal mechanisms, respectively, during the 2007 episode (M > 5, source Global CMT catalogue), and the largest beach ball indicates the main shock of focal mechanism (M 5.9). Red and blue rectangles mark the imaged area by ALOS/PALSAR (cf. Table 1).

besides the dike intrusion, and examined the details of the dike intrusion processes using the high temporal resolution SAR data. Baer et al. (2008) examined the Coulomb stress changes associated with the event to study the interaction of each fault source. Biggs et al. (2009) studied the relationship between the length of dike and the size of magma chamber compared with those in Afar and Iceland events. In regard to the relationship between the Oldoinyo Lengai eruption and the swarm, Baer et al. (2008) considered that the passage of the seismic-wave through the magma chamber could dynamically trigger the eruption, whereas Biggs et al. (2009) reported that there was no relationship between the eruption and the swarm due to the ground deformation spanning 2001–2004 implies no significant pressure changes in the magma chamber. Thus, the interrelation between the eruption and the event is still uncertain.

The objectives of this paper are to report the three-dimensional (3D) displacement fields that have never been reported by the previous studies and to show our source modeling results. This was made possible by a couple of reasons. Firstly, in contrast to the previous studies, we used L-band ALOS/PALSAR images acquired from both ascending and descending tracks. The L-band SAR is more advantageous in terms of the easiness of phase unwrapping even the areas with large phase gradient. Secondly, we apply both InSAR and offset-tracking methods that can reveal the full 3D displacements. Based on the inferred fault slip model, we also discuss the implications for the regional stress field and their possible role for the generation of fault segmentation along the rift axes. Moreover, we point out the possibility of the aseismic slip as the driver of earthquake swarm.

2. Data processing and SAR observation

Satellite-based SAR is helpful to obtain ground surface deformation signals with unprecedented spatial resolution over wide areas (e.g., Hanssen et al., 2001; Massonnet and Feigl, 1998). We detected the deformation signals associated with the 2007 event using both ascending and descending ALOS/PALSAR (L-band, 23.6 cm wave length) images (Table 1), providing us with the range changes along the radar line of sight (LOS) from two independent directions.

We also applied the offset-tracking method to derive the displacements projected along the satellite flight direction. We could thus derive the 3D displacements associated with the entire episode. The off-nadir angles are 34.3° for both tracks. The ascending data set (7 July 2007 to 7 October 2007) and the descending data set (5 June 2007 to 13 June 2010) cover the entire swarm period (Fig. 1). While the temporal coverage of the descending InSAR image is much longer than that of the ascending InSAR image, because no descending images were acquired between July 2007 and June 2010, and the descending InSAR could include post-seismic deformation signals. However we confirmed insignificant deformation signals after October 2007 from the ascending post-seismic interferogram (7 October 2007 to 15 July 2010) that revealed very little deformation (Fig. S2). To remove the topographic fringes in InSAR data, we used the 3 arc-second (90 m) Shuttle Radar Topography Mission (SRTM) digital elevation model (DEM) (Farr et al., 2007). SAR data were processed by GAMMA software (Wegmüller and Werner, 1997). Although we corrected for the orbital and topographic fringes with the use of precision orbit data by JAXA and SRTM DEM, respectively, there still remain long-wavelength phase trends and topography-correlated fringes. The effects of long-wavelength trend and topographic-correlated atmospheric delay in the interferograms were removed, by fitting low-order polynomials and DEM, respectively. For phase unwrapping, we used the branch-cut algorithm (Goldstein

Table 1
The ALOS/PALSAR data sets in this study.

Pair No.	Date (yyyy/mm/dd)	Orbit	Path	Frame	Bperp [m]
1	2007/07/07–2007/10/07	Ascending	568	7130	−249.05
2	2007/06/05–2010/06/13	Descending	236	3670–3680	−396.21

et al., 1988). While the unwrapping error would appear at different locations in the ascending and descending data, we confirmed that the phase discontinuities were observed at the same locations, suggesting that they are real deformation signals.

The observed InSAR data for both ascending and descending tracks are shown in Fig. 2a and d. They are resampled with the quad-tree algorithm to effectively reduce the number of data points from ~25,000 to ~4000 (Jonsson et al., 2002). The two interferograms indicate two clear phase discontinuities around the center of the graben that strike NE–SW (36.10E, 2.66S–36.01E, 2.77S) and NNW–SSE (36.05E, 2.63S–36.05E, 2.71S). We also identify another phase discontinuity to the NE that is particularly clear in Fig. 2a. The area between the two discontinuities indicates an increase in the radar line of sight (LOS) in both ascending (Fig. 2a) and descending data (Fig. 2d), suggesting that the area has subsided. In contrast, outside this region the signal in the ascending and descending data is opposite, suggesting E–W motion (Fig. 2a and d). We can thus roughly interpret that the LOS-increasing area was subsiding, and that the outer eastern and western areas were moving to the east and west, respectively. The interferograms indicate that the subsidence area covers 3–4 km width and 13–15 km length. The maximum positive range changes are 46 and 63 cm in ascending and descending data, respectively. Overall, the spatial pattern of the deformation signals looks like a graben structure, which has been reported at other rifting episodes such as the 2009 western Arabia, the 2007 Dallol, and the 1998 Réunion island (Baer and Hamiel, 2010; Fukushima et al., 2010; Nobile et al., 2012). As shown below, however, the azimuth offset data exhibit some unexpected signals.

Azimuth offset data derived from the ascending path similarly indicates two discontinuities (Fig. 3a) that are compatible with the expanding areas with E–W motion in the interferograms (Fig. 2a and d). The most remarkable point is that the subsiding zone indicates ~40 cm negative offset, which indicates that the area has moved opposite to the satellite flight direction. Namely, the central subsiding region was not only subsiding but also moving horizontally, because the azimuth offsets have no sensitivities to the vertical displacements. Although the azimuth offset derived from the descending pair is much noisier due to the lower-coherence, the data set also exhibits small horizontal displacements that are nearly in parallel with the satellite flight direction (Fig. S1). The azimuth offset data from both ascending and descending tracks thus unambiguously indicate horizontal displacements of a subsiding graben structure. Biggs et al. (2009) showed a result from multiple aperture InSAR (MAI) measurement (Bechor and Zebker, 2006), which are quite consistent with Fig. 3a in terms of both the signal amplitude and the deforming area. Nevertheless, they dismissed the MAI observation in their analyses, probably because there were no other independent data that could support the signal.

We calculated 3D displacements from the ascending and descending interferograms and the azimuth offset (Fig. 5a) (Fialko et al., 2001). The orange lines in Fig. 4 show the locations for the top edges of our fault source models shown below. The interval of the observation point is 2 × 2 km. The lack of the points around the summit of Mt. Gelai is because the azimuth offsets are noisier than the InSAR data and thus such area are masked. The horizontal displacements in Fig. 5a indicate that the western and the eastern half of the areas moved up to ~35 cm toward W–WSW and ~51 cm toward E–NE, respectively. The subsidence zone moved toward SSW direction with a maximum horizontal displacement of ~48 cm. The vertical displacements are shown in Fig. 5b, which indicates that the eastern half was uplifting and the center area was subsiding by ~62 cm. In contrast, the western half was uplifting by only a few centimeters.

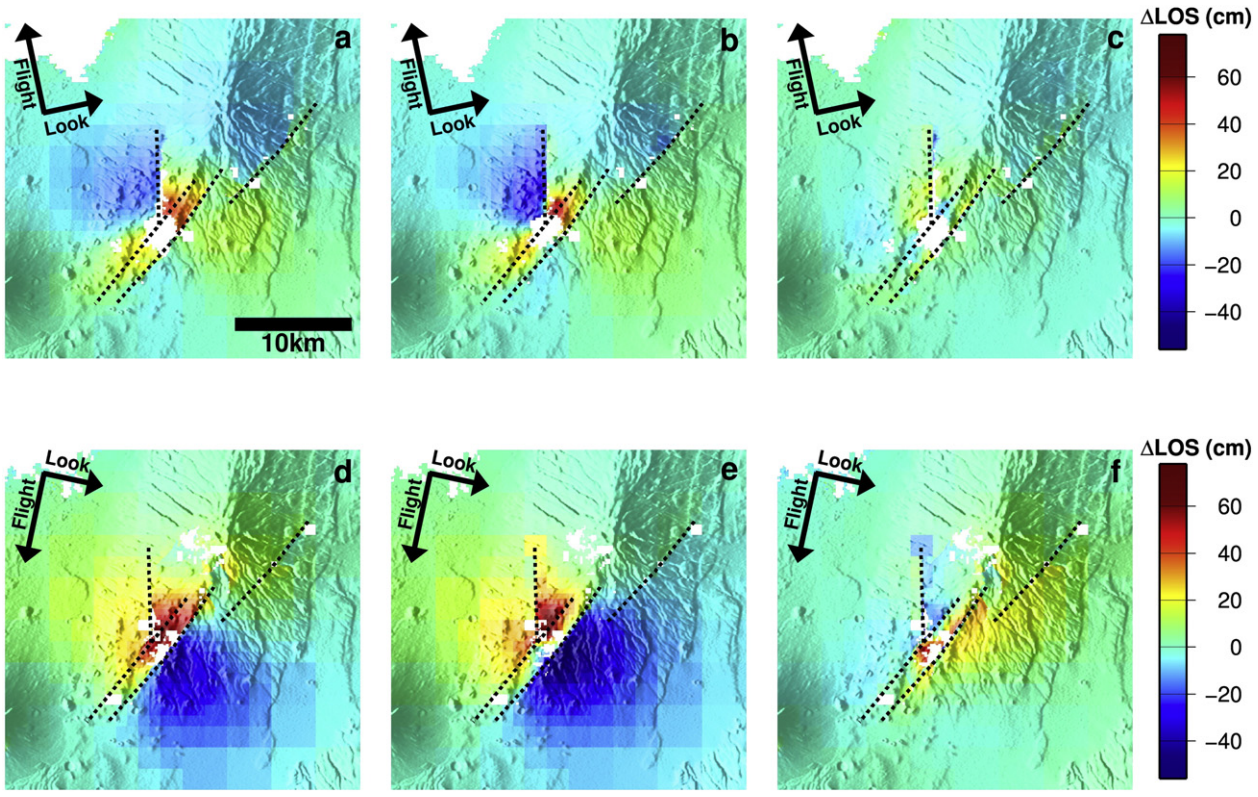

Fig. 2. (a, d) Observed unwrapped interferograms covering the 2007 event derived from (a) ascending and (b) descending tracks. (b, e) Calculated interferograms from the inferred fault slip distribution in Fig. 6 for (b) ascending and (e) descending. (c, f) Misfit residuals between the observed and calculated for (c) ascending and (f) descending. The unit vector of line of sight is $(e_e, e_n, e_z) = (0.613, 0.131, -0.779)$ for ascending and $(e_e, e_n, e_z) = (-0.612, 0.131, -0.780)$ for descending, respectively. Black dot lines indicate the top of the faults. Two arrows in each figure indicate the satellite flight direction and beam radiation direction.

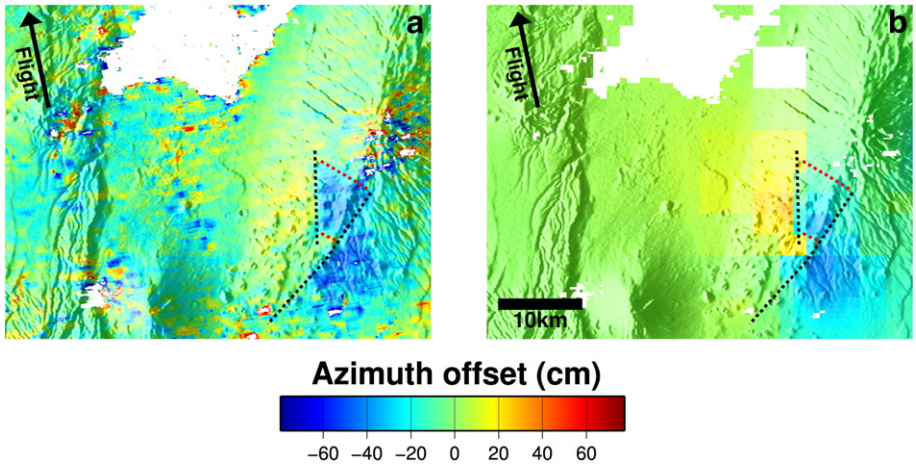

Fig. 3. (a) Observed azimuth offset derived from the ascending pair. (b) Calculated azimuth offset from the estimated slip distributions in the estimated from fault source modeling. Black dashed lines mark the top of the two facing faults. The two phase discontinuities along the direction orthogonal to the fault strike are indicated by the red dashed lines. The arrow in the top left indicates the flight direction of the satellite, and the unit vector is $(e_e, e_n, e_z) = (-0.209, 0.978, 0)$.

3. The elastic dislocation source modeling

Static ground displacements associated with earthquakes and/or dike intrusion episodes are often interpreted by using analytical solutions due to planar rectangular dislocation elements in elastic half-space (Okada, 1985). In this study, we estimate non-planar fault planes based on the analytical solutions due to triangular dislocation elements because the observations reveal complex deformation signals. The triangular dislocation elements are advantageous because it can represent non-planar fault planes without making unrealistic overlaps or gaps (Furuya and Yasuda, 2011; Maerten et al., 2005). To calculate the ground deformation due to the triangular dislocation elements, we use the MATLAB script that is made available by Meade (2007). To generate the mesh coordinates for the non-planar planes, we used Gmsh software (Geuzaine and Remacle, 2009).

Almost all the focal mechanisms of the earthquakes during the event show normal faulting. We set a west-dipping and an east-dipping fault whose top edges can match the locations off the phase discontinuities in the interferograms (Figs. 4, 6); the other parameters for the fault geometry, the bottom location and depth, were estimated by trial-and-errors (e.g., Furuya and Yasuda, 2011). We set another west-dipping fault at the eastern flank of Mt. Gelai (Fig. 6e–f), because the two interferograms indicate a phase discontinuity at the same location. The deformation pattern is consistent with a dike intrusion and can be modeled as a tensile opening dislocation source. We set a vertical tensile dislocation source as the dike segment, whose horizontal location is the center of the subsidence zone. Without dike opening, we could have only reproduced the subsidence zone with smaller E–W extension displacement. The final position of the dike segment was set where the RMS misfit was minimum. We thus estimated three faults and one dike segment to explain the crustal deformation (Fig. 5). Our model is similar to the geometry of Baer et al. (2008), regarding an east-dipping fault, two west-dipping faults and a dike segment. After setting the location and geometry of the fault sources and dike, we performed a linear least squares inversion to derive the spatially variable slip and opening on the fault and dike, inverting jointly the ascending and descending interferograms. Here we do not invert for the azimuth offset data, and instead we check the consistency a posteriori as argued below. In solving the least squares problem, we applied a "non-negativity" constraint. Namely, in order to derive physically plausible slip distributions, we prescribed that the east-dipping and west-dipping faults are allowed to slip right-laterally and left-laterally, respectively, and that the dip

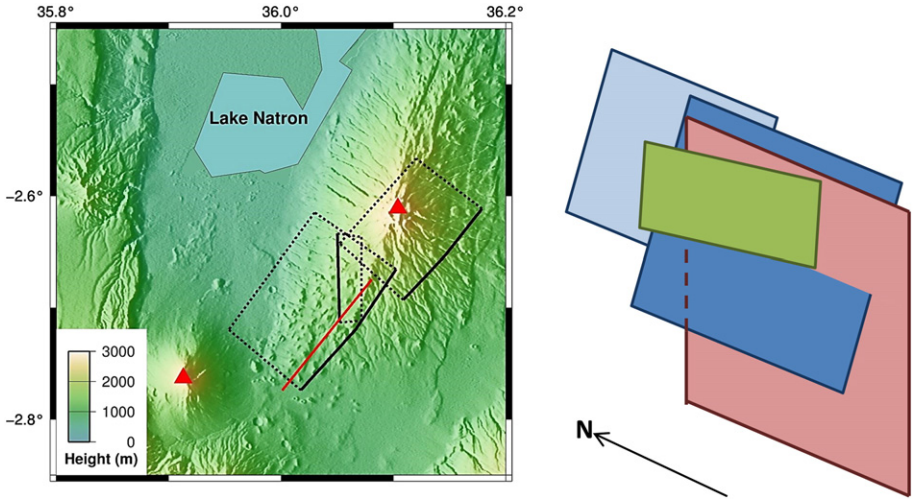

Fig. 4. Surface projection and 3D display of the fault model geometry. (Left) Solid lines mark the top edge of the faults, and the dashed lines indicate the side and bottom edges of the faults. Red indicates the location of the dike segment. (Right) Blue segments indicate east-dipping faults, green segment is east-dipping fault, and red segment is dike. The inferred slip distributions are shown in Fig. 6.

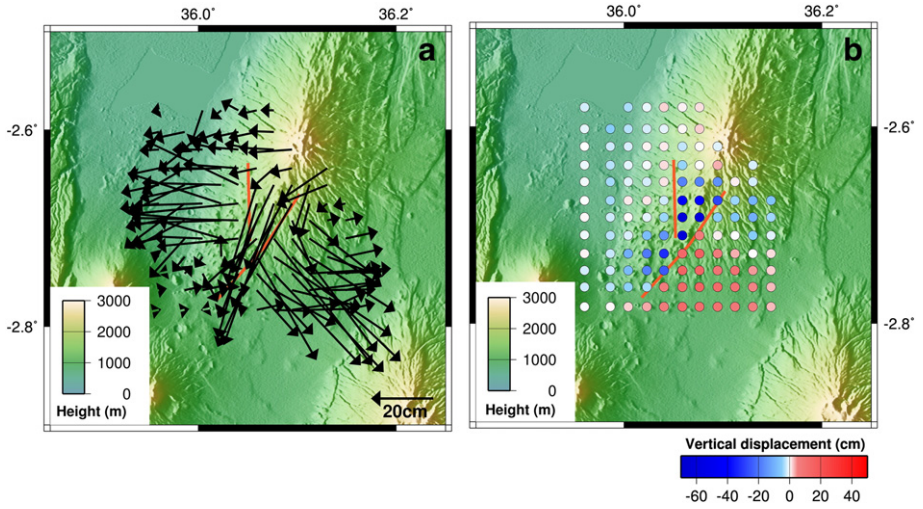

Fig. 5. Inferred 3D displacement using both ascending and descending interferograms and the azimuth offset tracking in the azimuth direction. (a) Horizontal displacements. (b) Vertical displacements. Orange lines in each figure follow the top of the confronted faults.

slip on each segment has only normal slip component. The dike segment is allowed to have only pure opening. Moreover, we apply a smoothing constraint on the slip distribution by using an umbrella operator that is equivalent to the Laplacian operator for the rectangular dislocation elements (Maerten et al., 2005). The moment release from the fault slip distribution can be calculated, assuming Poisson ratio of 0.25 and shear modulus of 30 GPa.

The optimum fault slip and dike opening distribution on each segment are shown in Fig. 6. Each fault slip distribution has maximum amplitude around the depth of ~5 km with their amplitudes up to 60 cm in the strike–slip and 160 cm in the dip slip. As expected from the Global CMT solutions that indicate predominantly normal faulting, the normal slip is much larger than the strike–slip (Fig. 6b, d). However, the inferred strike–slip component is unexpectedly larger than that inferred by seismology (Fig. 6a, c). The calculated geodetic moment for the dip slip component is 3.3×10^{18} Nm, and that for the strike–slip component is 8.1×10^{17} Nm. Thus, the contribution of the strike–slip is 19.9%, and the equivalent moment magnitude for the dip slip and strike–slip is Mw 6.28 and 5.87, respectively. Because the cumulative seismic moment is 2.2×10^{18} Nm according to the Global CMT, it turns out that about 56% of the geodetic moment were released aseismically. The moment for the strike–slip must be responsible for the southward movement of the subsidence zone. The dike segment exhibits up to 220 cm opening at the depth of 2–4 km (Fig. 6g), and the volume of intrusion is 0.036 km^3.

While we may include a Mogi-type deflation source to account for the source of the intruded dike, we cannot identify any circular signals in the observed InSAR data that allows us to constrain such a source. Although we do not discard the presence of a deflation source, we consider that the depth of the Mogi source, if any, would be deeper than 3 km, because otherwise there would arise circular fringes; we then assumed that the Mogi source has the same volume changes as those of intruded dike. Moreover, even if we include the deflation source at the center of the largest displacement field, the E–W trending sharp offset at northern and southern edge of the negative signal will never be generated.

Based on the inferred fault slip and dike opening distribution, we computed the ground deformation (Fig. 2b, e) and misfit residual (Fig. 2c, f). RMS residual values in our model are 3.0 cm in the ascending and 6.3 cm in the descending data. Although there still remain some residuals in the eastern half of the descending data, the calculated deformation well reproduces the observations, and the misfit residuals cannot be distinguished from measurement errors that would be empirically less than 5 cm for a single interferogram. Also, we calculated the displacements for the azimuth offset, which also reproduces the characteristic offsets in the subsidence zone (Fig. 3).

Without the strike–slip component, we could not reproduce the large azimuth offset signals in the subsidence zone. Thus we conclude that the strike–slip is necessary to explain the observation results, and it occurred aseismically because almost all the Global CMT solution exhibits the normal-dip slip.

4. Discussion

To our knowledge, not only the previous studies of the 2007 Lake Natron event, but also many studies of dike intrusion events in rift settings elsewhere assume normal slip and dike opening in their fault source modeling (e.g., Baer and Hamiel, 2010; Hamling et al., 2014; Nobile et al., 2012; Wright et al., 2006). Focal mechanisms of earthquakes during the 2007 event indeed indicate few strike–slip components. In contrast, the fault source model we estimated in this study includes significant strike components, without which we cannot reproduce the InSAR and azimuth offset observations. Considering the few strike–slip in the focal mechanisms, it turns out that aseismic strike components are required to explain the ground deformation associated with the 2007 Natron event. Why then did the aseismic strike–slip occur at the area that is supposed to extend in the E–W direction? Why did the subsiding area move toward the south that is orthogonal to the rift axis?

In order to examine if the stress changes due to the dike intrusion promoted the fault slips, we computed the Coulomb stress changes (ΔCFF), based on the our inferred fault models (e.g., King et al., 1994; Toda et al., 2002). In the calculations of the ΔCFF, we use a shear modulus of 30 GPa and a friction coefficient of 0.4. Fig. 7 illustrates the distribution of the ΔCFF by the dike opening for each receiver fault at depths from the surface to 6 km. We observe positive values of ~0.05 MPa at shallower depths, suggesting unclamping, mainly distributed along the dike axis (Fig. 7a–f). In the meantime, at the depths of 2–4 km at which we inferred the peak values of dike opening, the negative ΔCFF (clamping) are widely distributed (Fig. 7j–r). Our inferred fault models indicate significant slip distributions mostly at shallower depths, and thus are mechanically consistent with the ΔCFF.

In the above ΔCFF modeling, however, we do not consider the background tectonic stress fields. The two west-dipping faults are forming en-echelon structure, and the strike components are much larger than the normal slip at the shallower depth of the west-dipping fault to the northeastern end. There are many normal fault systems in the EAR,

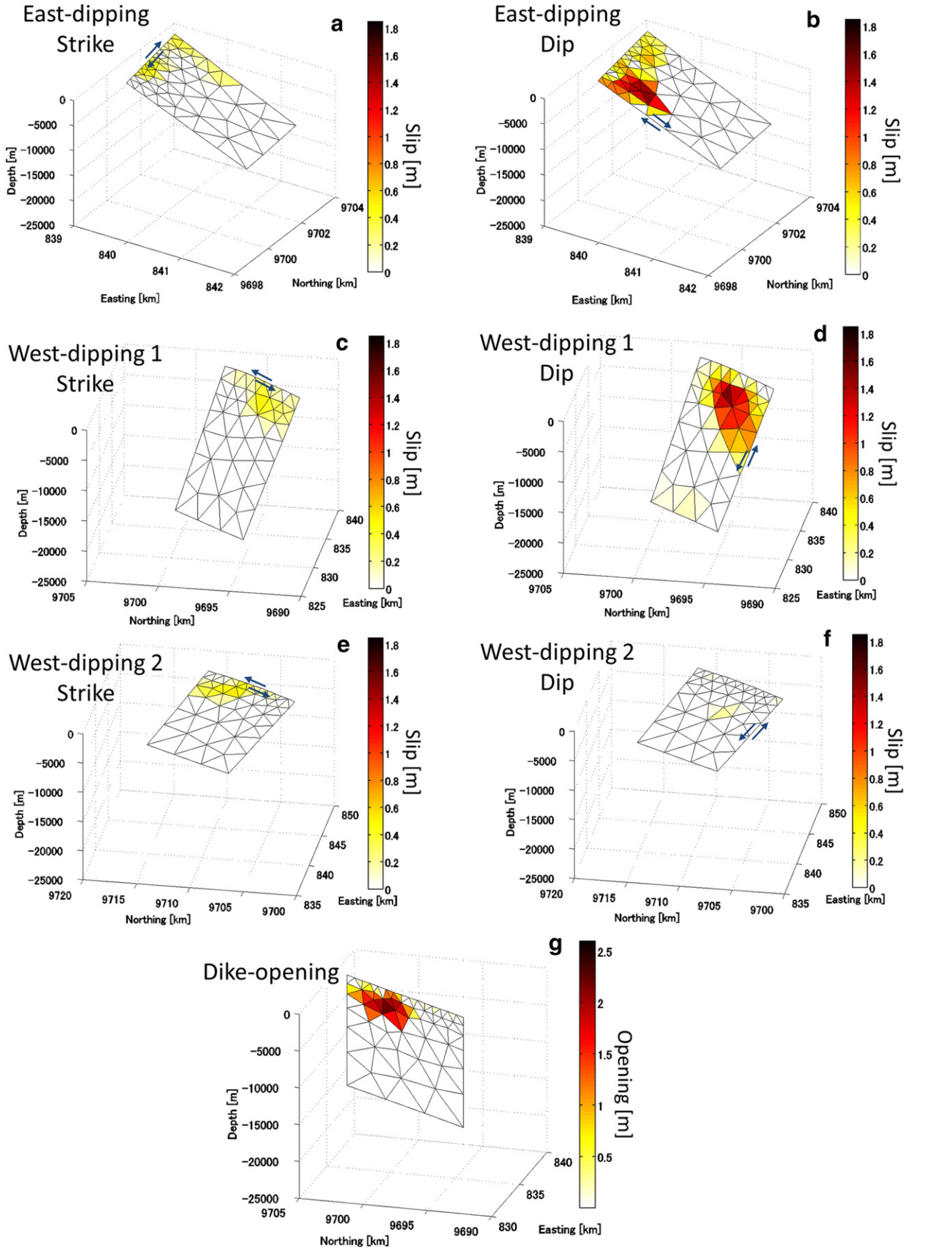

Fig. 6. Estimated slip distribution for each segments. See the texts for details. (a, b) Slip distributions were shown on the east-dipping fault. (c, d) West-dipping fault 1 is one of the confronted faults. (e, f) West-dipping fault 2 located at the eastern flank of Mt. Gelai. Slip direction is shown as vector in the figures. (g) Dike was imposed pure opening. The arrows indicate slip directions of each of the faults. The unit of dislocation or opening is indicated with a metre scale. The rake angle for each angle is −77.6, −100.1, and −167.6 degrees measures clockwise from the north in the east-dipping, west-dipping 1, and west-dipping 2 fault, respectively.

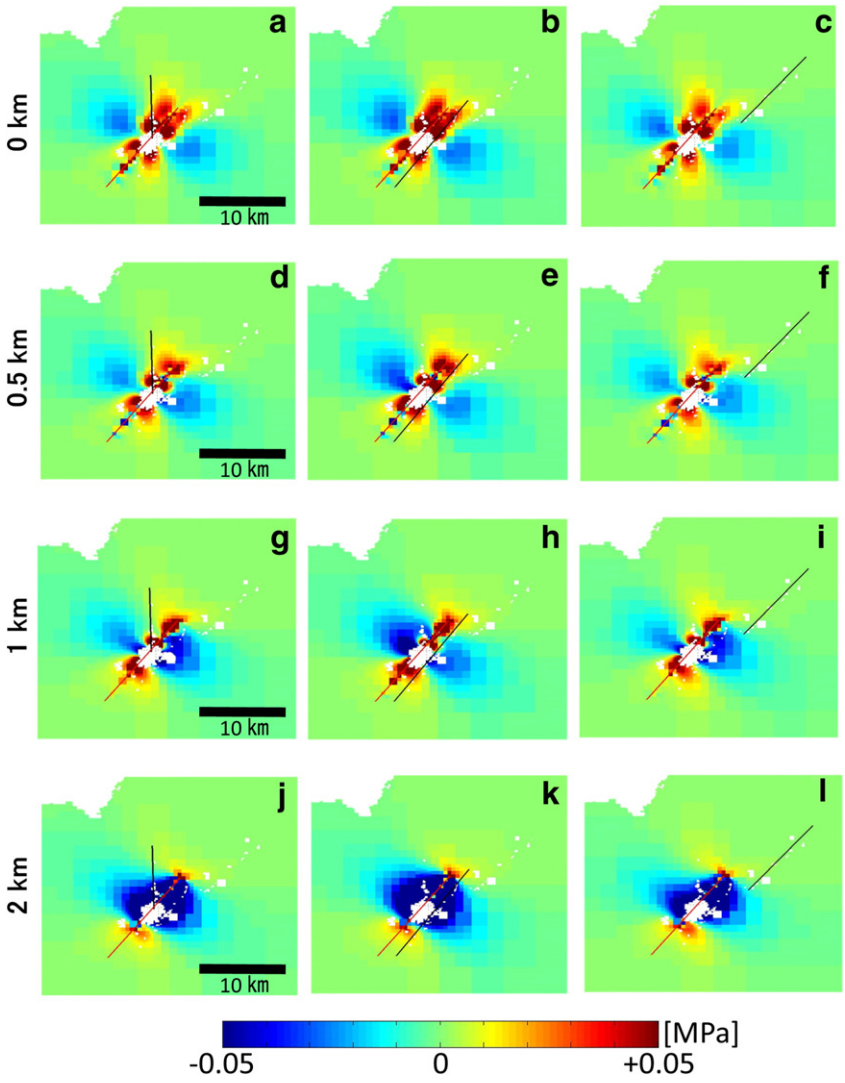

Fig. 7. Coulomb stress changes for the receiver faults (black lines) due to the dike opening as the source fault (red line). The top edges of the receiver faults are shown as black lines (left column: east-dipping fault, center: west-dipping fault, right: shallow west-dipping fault). Stress changes indicate positive (unclamping) the near surface, and the most negative (clamping) at the depth of maximum dike opening around 2–3 km.

which are forming relay zones and segmented structures (Ebinger, 1989; Moustafa, 2002; Tesfaye et al., 2008). Relay zone is a geological structure formed by multiple overlapping, en-echelon fault segments and develops under a transtensive stress field instead of pure extension (Crider and Pollard, 1998).

The background stress field around the Lake Natron has been estimated from the focal mechanisms of past earthquakes (Delvaux and Barth, 2010; the World Stress Map available online at http://www.world-stress-map.org). Those studies indicate a pure extension stress regime toward NNW–SSE around the Lake Natron. The NNW–SSE axis is consistent with the orthogonal direction of the main shock strike direction during the 2007 event. Moreover, Delvaux and Barth (2010) and the World Stress Map indicate ENE–WSW pure extensive stress field in the Lake Manyara region, which is located 50 km to the south from the 2007 Natron rifting event area.

The stress field estimated from seismological studies, however, indicates seismotectonic stresses, and the stress field can change at the other depths than the depth of the employed hypocenters. It is likely that the existence of a microplate or magma intrusion can build up a three-dimensionally complicated stress field. As shown in the slip distribution in Fig. 6, the strike–slip is dominating at the shallower depth, suggesting the transcurrent stress regime. Meanwhile, it is well-known that the shallowest zone of the crust exhibits a velocity-strengthening tendency in the friction parameters of the rate-and-state dependent friction law, meaning the absence of seismic slip and the presence of aseismic slip (Scholz and Contreras, 1998). In other words, it should be noted that we cannot infer a true stress regime at the shallowest depths from seismological studies, no matter what type of stress fields are dominant. Thus we may claim that this study is the first to have confirmed the transtensive stress regime at shallower depth around the Lake Natron by the detection of the aseismic strike–slip based on the InSAR data. Although Wright et al. (2006) suggested that dike intrusion is essential to form the along-axis segmentation, and we do not dispute its importance, our detection of significant strike–slip at shallow depth is a direct evidence for the presence of transtensive stress that is necessary to generate the along-axis segmentation like relay zone (transfer zone). We consider that the dike intrusion could contribute to generate the three-dimensionally complex stress distributions. Since our dike opening model sets a kinematic displacement boundary condition instead of stress boundary condition, we should note that the stress axis around the study area does not have to coincide with the dike opening direction.

The relay ramp is known to form between antithetic normal faults like graben structure (Amer et al., 2012; Tesfaye et al., 2008). As the relay ramp develops, a fracture can be built up along the direction orthogonal to the fault strike direction, generating new normal faults as transfer faults (Commins et al., 2005; Xu et al., 2011). Such fractures

are also observed at the Northern Lake Rukwa (Chorowicz, 2005). While we do not include it in the source model of this study, we can identify such discontinuities in the azimuth offset observation as indicated by the red dashed line (Fig. 3). We consider that those discontinuities would also be the evidence for the horizontal motion of the subsiding region.

The observed aseismic slip may also have an important implication for generation of earthquake swarm (e.g., Lohman and McGuire, 2007; Takada and Furuya, 2010; Wicks et al., 2011). Earthquake swarm is often attributed to fluid or magma intrusion, and it is apparent that such an intrusion occurred during our studied period. However, besides the dike intrusion process, aseismic slip has been proposed as another possible driver of swarm episode. We may regard the detected aseismic strike–slip as another evidence for the proposed swarm mechanism.

5. Conclusion

Using ALOS/PALSAR data, we have detected the ground displacements associated with the 2007 northern Tanzanian earthquake swarm episode near the Lake Natron. In addition to the two-pass InSAR data from both ascending and descending paths, we derived azimuth offset data that are sensitive to the displacements parallel to the satellite flight direction. We could thus demonstrate the 3D displacement fields. Besides the graben-like structure already pointed out in the previous studies, the 3D displacement fields indicate that the subsidence zone moved toward SSW.

Our fault source model consists of one tensile-opening fault, one east-dipping fault, and two west-dipping faults. One notable difference of our fault model from previous studies is the presence of strike–slip component that turns to contribute to approximately 20% of the whole moment release. Because the focal mechanisms of the earthquakes during the 2007 swarm event represent nearly pure normal faulting, we consider that aseismic strike–slip on the faults is responsible for the horizontal movement of the subsidence zone.

Supplementary data to this article can be found online at http://dx.doi.org/10.1016/j.tecto.2015.06.005.

Acknowledgement

We generated all of the interferograms and pixel-offset data from Phased Array-Type L-Band Synthetic Aperture Radar (PALSAR) level 1.0 data, using the commercial software package from GAMMA Remote Sensing. PALSAR level 1.0 data used in this study are shared among the PALSAR Interferometry Consortium to Study our Evolving Land surface (PIXEL), and provided by JAXA under a cooperative research contract with the Earthquake Research Institute, University of Tokyo. The ownership of PALSAR data belongs to JAXA and the Ministry of Economy, Trade and Industry (METI). The Global Centroid Moment Tensor Project database was searched using www.globalcmt.org/CMTsearch.html (last accessed on July 2014). Some of the figures in this paper were made by Matlab (http://www.mathworks.com, last accessed on January 2015). Some figures were prepared using the public domain Generic Mapping Tools (GMT). We thank the anonymous reviewer and the Editor for their careful reading and comments, which we believe were helpful to improve the original manuscript.

References

Albaric, J., Perrot, J., Déverchère, J., Deschamps, A., Le Gall, B., Ferdinand, R.W., Petit, C., Tiberi, C., Sue, C., Songo, M., 2010. Contrasted seismogenic and rheological behaviours from shallow and deep earthquake sequences in the North Tanzanian Divergence, East Africa. J. Afr. Earth Sci. 58, 799–811. http://dx.doi.org/10.1016/j.jafrearsci.2009.09.005.

Amer, R., Mohamed, S., Robert, R., John, E., 2012. Structural architecture for development of marginal extensional sub-basins in the Red Sea Active Rift Zone. Int. J. Geosci. 2012, 133–152.

Aoki, Y., Segall, P., Kato, T., Cervelli, P., Shimada, S., 1999. Imaging magma transport during the 1997 Seismic Swarm off the Izu Peninsula, Japan. Science 286, 927–930. http://dx.doi.org/10.1126/science.286.5441.927.

Baer, G., Hamiel, Y., Shamir, G., Nof, R., 2008. Evolution of a magma-driven earthquake swarm and triggering of the nearby Oldoinyo Lengai eruption, as resolved by InSAR, ground observations and elastic modeling, East African Rift, 2007. Earth Planet. Sci. Lett. 272, 339–352. http://dx.doi.org/10.1016/j.epsl.2008.04.052.

Baer, G., Hamiel, Y., 2010. Form and growth of an embryonic continental rift: InSAR observations and modelling of the 2009 western Arabia rifting episode. Geophys. J. Int. 182, 155–167. http://dx.doi.org/10.1111/j.1365-246X.2010.04627.x.

Bechor, N.B.D., Zebker, H.A., 2006. Measuring two-dimensional movements using a single InSAR pair. Geophys. Res. Lett. 33, L16311.

Biggs, J., Amelung, F., Gourmelen, N., Dixon, T.H., Kim, S., 2009. InSAR observations of 2007 Tanzania rifting episode reveal mixed fault and dyke extension in an immature continental rift. Geophys. J. Int. 179, 549–558. http://dx.doi.org/10.1111/j.1365-246X.2009.04262.x.

Calais, E., D'Oreye, N., Albaric, J., Deschamps, A., Delvaux, D., Déverchère, J., Ebinger, C., Ferdinand, R.W., Kervyn, F., Macheyeki, A.S., Oyen, A., Perrot, J., Saria, E., Smets, B., Stamps, D.S., Wauthier, C., 2008. Strain accommodation by slow slip and dyking in a youthful continental rift, East Africa. Nature 456, 783–788.

Chorowicz, J., 2005. The East African rift system. J. Afr. Earth Sci. 43, 379–410. http://dx.doi.org/10.1016/j.jafrearsci.2005.07.019.

Commins, D., Gupta, S., Cartwright, J., 2005. Deformed streams reveal growth and linkage of a normal fault array in the Canyonlands graben, Utah. Geol. Soc. Am. 33, 645–648. http://dx.doi.org/10.1130/G21433.1.

Crider, J.G., Pollard, D.D., 1998. Fault linkage: three-dimensional mechanical interaction between echelon normal faults. J. Geophys. Res. 103, 24373. http://dx.doi.org/10.1029/98JB01353.

Delvaux, D., Barth, A., 2010. African stress pattern from formal inversion of focal mechanism data. Tectonophysics 482, 105–128. http://dx.doi.org/10.1016/j.tecto.2009.05.009.

Ebinger, C., 1989. Tectonic development of the western branch of the East African rift system. Geol. Soc. Am. Bull. http://dx.doi.org/10.1130/0016-7606(1989)101<0885.

Farr, T.G., Rosen, P., Caro, E., Crippen, R., 2007. The shuttle radar topography mission. Rev. Geophys. 45, 1–33. http://dx.doi.org/10.1029/2005RG000183.

Fialko, Y., Simons, M., Agnew, D., 2001. The complete (3-D) surface displacement field in the epicentral area of the 1999 Mw 7.1 Hector Mine earthquake, California, from space geodetic observation. Geophys. Res. Lett. 28, 3063–3066.

Fukushima, Y., Cayol, V., Durand, P., Massonnet, D., 2010. Evolution of magma conduits during the 1998–2000 eruptions of Piton de la Fournaise volcano, Réunion Island. J. Geophys. Res. 115, B10204. http://dx.doi.org/10.1029/2009JB007023.

Furuya, M., Yasuda, T., 2011. The 2008 Yutian normal faulting earthquake (Mw 7.1), NW Tibet: non-planar fault modeling and implications for the Karakax Fault. Tectonophysics 511, 125–133. http://dx.doi.org/10.1016/j.tecto.2011.09.003.

Geuzaine, C., Remacle, J.-F., 2009. Gmsh: a 3-D finite element mesh generator with built-in pre- and post-processing facilities. Int. J. Numer. Methods Eng. 79, 1309–1331. http://dx.doi.org/10.1002/nme.2579.

Global CMT, project at, http://www.globalcmt.org (Last accessed October 2014).

Goldstein, R.M., Zebker, H., a., Werner, C.L., 1988. Satellite radar interferometry: two-dimensional phase unwrapping. Radio Sci. 23, 713–720. http://dx.doi.org/10.1029/RS023i004p00713.

Hamling, I.J., Ayele, A., Bennati, L., Calais, E., Ebinger, C.J., Keir, D., Lewi, E., Wright, T.J., Yirgu, G., 2009. Geodetic observations of the ongoing Dabbahu rifting episode: new dyke intrusions in 2006 and 2007. Geophys. J. Int. 178, 989–1003. http://dx.doi.org/10.1111/j.1365-246X.2009.04163.x.

Hamling, I.J., Wright, T.J., Calais, E., Lewi, E., Fukahata, Y., 2014. InSAR observations of post-rifting deformation around the Dabbahu rift segment, Afar, Ethiopia. Geophys. J. Int. 1–17.

Hanssen, R.F., Feijt, A.J., Klees, R., 2001. Comparison of precipitable water vapor observations by spaceborne radar interferometry and Meteosat 6.7-μm. Radiometry 18, 756–764.

Jonsson, S., Zebker, H., Segall, P., Amelung, F., 2002. Fault slip distribution of the 1999 Mw 7.1 Hector Mine, California, earthquake, estimated from satellite radar and GPS measurements. Bull. Seismol. Soc. Am. 92, 1377–1389.

King, G.C.P., Stein, S., Lin, J., 1994. Static stress changes and the triggering of earthquakes. Bull. Seismol. Soc. Am. 84, 935–953.

Lohman, R.B., McGuire, J.J., 2007. Earthquake swarms driven by aseismic creep in the Salton Trough, California. J. Geophys. Res. 112, B04405. http://dx.doi.org/10.1029/2006JB004596.

Maerten, F., Resor, P., Pollard, D., Maerten, L., 2005. Inverting for slip on three-dimensional fault surfaces using angular dislocations. Bull. Seismol. Soc. Am. 95, 1654–1665. http://dx.doi.org/10.1785/0120030181.

Massonnet, D., Feigl, K.L., 1998. Radar interferometry and its application to changes in the Earth's surface. Rev. Geophys. 36, 441–500.

McKenzie, D., Davies, D., Molnar, P., 1970. Plate tectonics of the Red Sea and East Africa. Nature 226, 243–248.

Meade, B.J., 2007. Algorithms for the calculation of exact displacements, strains, and stresses for triangular dislocation elements in a uniform elastic half space. Comput. Geosci. 33, 1064–1075. http://dx.doi.org/10.1016/j.cageo.2006.12.003.

Moustafa, A., 2002. Controls on the geometry of transfer zones in the Suez rift and northwest Red Sea: implications for the structural geometry of rift systems. Am. Assoc. Pet. Geol. Bull. 6, 979–1002.

Nobile, A., Pagli, C., Keir, D., Wright, T.J., Ayele, A., Ruch, J., Acocella, V., 2012. Dike–fault interaction during the 2004 Dallol intrusion at the northern edge of the Erta Ale Ridge (Afar, Ethiopia). Geophys. Res. Lett. 39. http://dx.doi.org/10.1029/2012GL053152.

Okada, Y., 1985. Surface deformation due to shear and tensile faults in a half-space. Bull. Seismol. Soc. Am. 75, 1135–1154.

Paquet, F., Dauteuil, O., Hallot, E., Moreau, F., 2007. Tectonics and magma dynamics coupling in a dyke swarm of Iceland. J. Struct. Geol. 29, 1477–1493. http://dx.doi.org/10.1016/j.jsg.2007.06.001.

Saria, E., Calais, E., Stamps, D.S., Delvaux, D., Hartnady, C.J.H., 2014. Present-day kinematics of the East African Rift. J. Geophys. Res. Solid Earth 3584–3600 http://dx.doi.org/10.1002/2013JB010901.

Scholz, C., Contreras, J., 1998. Mechanics of continental rift architecture. Geology 26, 967–970.

Stamps, D.S., Calais, E., Saria, E., Hartnady, C., Nocquet, J.M., Ebinger, C.J., Fernandes, R.M., 2008. A kinematic model for the East African Rift. Geophys. Res. Lett. 35, L05304. http://dx.doi.org/10.1029/2007GL032781.

Takada, Y., Furuya, M., 2010. Aseismic slip during the 1996 earthquake swarm in and around the Onikobe geothermal area, NE Japan. Earth Planet. Sci. Lett. 290, 302–310. http://dx.doi.org/10.1016/j.epsl.2009.12.024.

Tesfaye, S., Rowan, M.G., Mueller, K., Trudgill, B.D., Harding, D.J., 2008. Relay and accommodation zones in the Dobe and Hanle grabens, central Afar, Ethiopia and Djibouti. J. Geol. Soc. Lond. 165, 535–547. http://dx.doi.org/10.1144/0016-76492007-093.

Toda, S., Stein, R.S., Sagiya, T., 2002. Evidence from the AD 2000 Izu islands earthquake swarm that stressing rate governs seismicity. Nature 419, 58–61. http://dx.doi.org/10.1038/nature00997.

Wegmüller, U., Werner, C.L., 1997. Gamma SAR processor and interferometry software. Proc. of the 3rd ERS Symposium, European Space Agency Special Publication, ESA SP-414, Florence, Italy, pp. 1686–1692 (14–21 March 1997).

Wicks, C., Thelen, W., Weaver, C., Gomberg, J., Rohay, A., Bodin, P., 2011. InSAR observations of aseismic slip associated with an earthquake swarm in the Columbia River flood basalts. J. Geophys. Res. 116. http://dx.doi.org/10.1029/2011JB008433.

World Stress Map, d. at, http://www.world-stress-map.org (Last accessed November 2014).

Wright, T.J., Ebinger, C., Biggs, J., Ayele, A., Yirgu, G., Keir, D., Stork, A., 2006. Magma-maintained rift segmentation at continental rupture in the 2005 Afar dyking episode. Nature 442, 291–294. http://dx.doi.org/10.1038/nature04978.

Xu, S., Ángel Francisco, N.-S., Susana, A.A.-Á., Luis, M.C.-M., 2011. Structural analysis of a relay ramp in the Querétaro graben, central Mexico: implications for relay ramp development. Rev. Mex. 28, 275–289.